Available online at www.sciencedirect.com
ScienceDirect
Journal of the European Ceramic Society 30 (2010) 215–220
www.elsevier.com/locate/jeurceramsoc

On the localized impedance spectroscopic characterization of grain boundaries: General aspects and experiments on undoped $SrTiO_3$

J. Fleig [a,b,*], B. Rahmati [c], S. Rodewald [b], J. Maier [b]

[a] *Institute of Chemical Technologies and Analytics, Vienna University of Technology, Getreidemarkt 9-164/EC, 1060 Vienna, Austria*
[b] *Max Planck Institute for Solid State Research, Heisenbergstr. 1, 70569 Stuttgart, Germany*
[c] *Max Planck Institute for Metal Research, Heisenbergstr. 3, 70569 Stuttgart, Germany*

Available online 8 May 2009

Abstract

Impedance measurements using microelectrodes on adjacent grains of polycrystals are a valuable tool for a detailed analysis of grain boundary properties of ceramic materials. In order to support proper interpretation of such experiments two fundamental aspects are discussed in the theoretical part of this paper: first, it is shown that "localized" experiments using contact pads are often not reasonable and can lead to severe misinterpretation. Second, results from finite element calculations illustrate as to how far conclusions on the grain boundary resistivity distribution can be drawn from a measured grain boundary resistance statistics. In the experimental part, microelectrode impedance measurements and orientation imaging data on undoped polycrystalline $SrTiO_3$ are presented and interpreted in terms of the homogeneity of the space charge potentials at grain boundaries.

Keywords: Impedance; Electrical conductivity; Perovskites; Grain boundaries

1. Introduction

In many electroceramic applications grain boundaries play an important or even a functional role. Grain boundaries with high resistivity, for example, are the functional heart of varistors and positive temperature coefficient (PTC) resistors[1] but disadvantageous if good transport properties are required. Thus the electrical properties of grain boundaries in electroceramic materials have been in the focus of interest for many years. Impedance spectroscopy is an important tool for investigating grain boundaries since it allows one, at least in idealized cases, to split the overall dc resistance into contributions from the grain interior, the grain boundaries and the electrodes. In real cases, however, a quantitative analysis of grain boundary impedances is often far from trivial[2–4] and, for example, electrical properties varying from boundary to boundary can impede sensible conclusions from conventional impedance measurements.[3] Information on the distribution of individual grain boundary resistivities would thus help in consistently interpreting grain boundary impedance data.

Microcontacts can be employed in order to obtain spatially resolved information on electrical properties and several papers report on the dc current–voltage (I–V) characteristics of single grain boundaries in semiconducting ceramics such as ZnO-varistors.[5–12] In materials with the grain boundary resistance being of the same order of magnitude as the bulk resistance impedance spectroscopy can again help identify different contributions of the total resistance measured between two microelectrodes. Therefore, recent papers also dealt with the impedance spectroscopic analysis of grain boundaries in Fe-doped $SrTiO_3$ or Mn–Zn-ferrites using microelectrodes.[13,14]

Finite element calculations on the impedance between microelectrodes can then help interpret local measurements.[15] Such simulations quantitatively showed how far other grain boundaries close to the investigated one also influence the measurement results. The calculations also revealed, for example, that in polycrystals with a comparatively broad distribution of grain boundary resistances usually only the weakly or moderately blocking grain boundaries are "visible" in experiments.

In this contribution additional information is given on the interpretation of "single" grain boundary measurements by means of microelectrodes: in Section 2 we consider the

* Corresponding author at: Institute of Chemical Technologies and Analytics, Vienna University of Technology, Getreidemarkt 9-164/EC, 1060 Vienna, Austria. Tel.: +43 158801 15800; fax: +43 158801 15899.
E-mail address: j.fleig@tuwien.ac.at (J. Fleig).

0955-2219/$ – see front matter © 2009 Elsevier Ltd. All rights reserved.
doi:10.1016/j.jeurceramsoc.2009.04.007

problem of using macroscopic contact pads for feeding the current. Section 3 deals with finite element calculations on the relation between the given grain boundary property distribution and the statistics of the measured grain boundary resistances. In Section 4 several aspects are exemplified in a study on the structure–property relationship of polycrystalline undoped $SrTiO_3$ investigated by microelectrode impedance measurements and orientation imaging microscopy.

2. Geometrical considerations

In several experimental studies on local grain boundary properties, large contact pads at the periphery of a sample have been employed to feed the current. As sketched in Fig. 1a, a connection line on the sample's surface is then used to connect contact pads and what is thought to be a microelectrode. However, such a set-up can be very problematic when investigating local properties since experimental results are, in many cases, determined by the current between the two large contact electrodes rather than by the current between the microelectrodes. This can be understood from the electrode configuration shown in Fig. 1b: extended electrodes on two sides of a square sample are used as current feed electrodes and very thin, highly conductive metal lines connect these large contacts to the circular microelectrodes on adjacent grains. In case of a single crystal (bulk conductivity σ_{bulk}) the resistance between two circular microelectrodes R_{me} of diameter d_{me} is given[13] by $(\sigma_{bulk} d_{me})^{-1}$ while the resistance R_c between the two contact electrodes simply reads $(\sigma_{bulk} h)^{-1}$ with h being the sample height. The resistance between the microelectrodes therefore typically exceeds the resistance between the current feed electrodes by one to three orders of magnitude and most of the current flows between the contact electrodes. Spatially resolved bulk conductivities cannot be deduced from such measurements.

For a polycrystalline sample with highly resistive, identical grain boundaries of conductivity σ_{gb}, the situation is very similar. The grain boundary resistance between the two microelectrodes on adjacent grains of grain size L_g is approximately given by $R_{gb,me} \approx 0.4 w_{gb}/(\sigma_{gb} L_g^2)$. (Symbol w_{gb} denotes the grain boundary thickness and the numerically determined factor of approximately 0.4 reflects the fact that a fraction of the current does not directly flow through the grain boundary between the two relevant grains but via neighboring grain boundaries, see also Section 3.)[15] The grain boundary resistance between the two extended contact electrodes is $R_{gb,c} \approx w_{gb}/(\sigma_{gb} L_g h)$. Thus, a resistance ratio $R_{gb,me}/R_{gb,c} \approx 0.4h/L_g$ results, and the measured grain boundary resistance is usually again dominated by the grain boundary resistance between the two large contacts. (For the sake of clarity the grains in Fig. 1b are unrealistically large.) Consequently, measurements using electrode configurations similar to that sketched in Fig. 1a and b are mostly macroscopic measurement and result in resistance and capacitance values which are typical for conventional impedance experiments, while true microelectrode measurements yield much higher resistances and much lower capacitances.

Only for grain boundaries between the microelectrodes being considerably less resistive than all others, meaningful data might result for electrode configurations similar to those in Fig. 1a and b. For example, this can be the case for voltages above the threshold voltage of a ZnO-varistor grain boundary. The resistance of the grain boundary between the microelectrodes then breaks down, while all other grain boundaries remain highly resistive and most of the current may indeed pass this single boundary. Contact pads which are insulated from the sample prevent a dc current between the pad electrodes and therefore facilitate reasonable dc microelectrode measurements. However, impedance measurements can still be severely impeded by capacitive currents across the insulating layer.

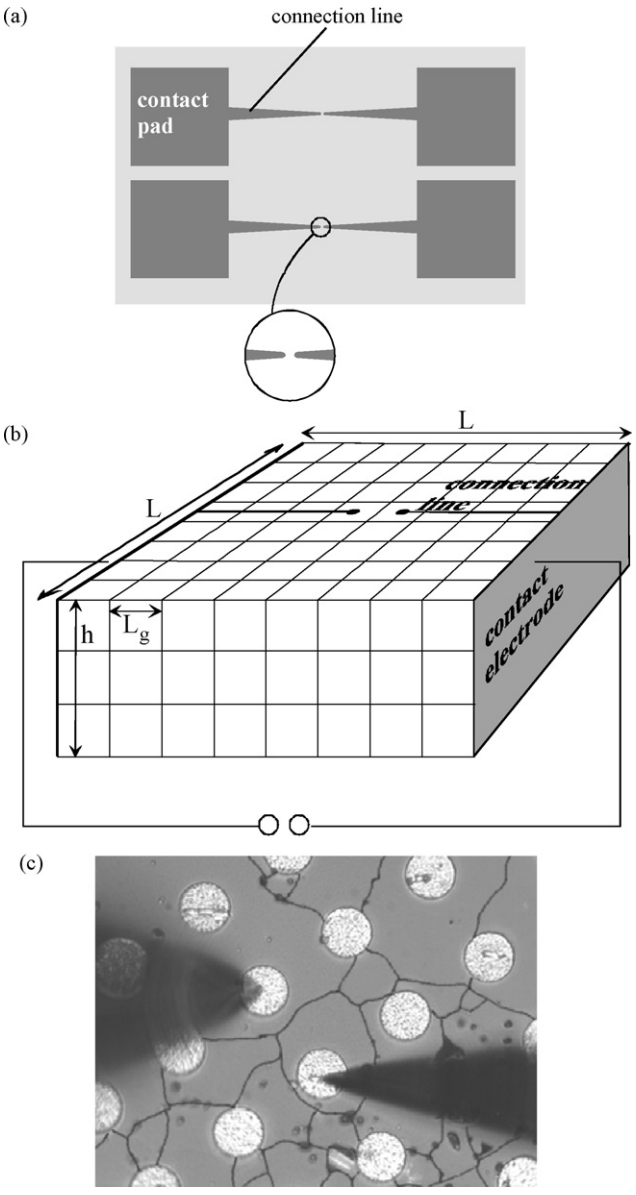

Fig. 1. (a) Electrode configuration sometimes used to perform "microelectrode" measurements. The end of a connection line is assumed to represent a microelectrode. (b) Sketch of a model sample with extended contact electrodes and very thin highly conductive connection lines to the circular "microelectrodes". (c) Image of circular microelectrodes on a $SrTiO_3$ polycrystal contacted under the optical microscope by contact tips.

Microelectrodes being directly contacted by contact tips are therefore recommended for spatially resolved grain boundary

measurements. A possible arrangement is shown in Fig. 1c (10 μm microelectrode pattern on $SrTiO_3$ contacted by movable contact tips). Nevertheless, one should keep in mind that the stray capacitance between two metallic contact needles (of the order of a few 10 fF) may still be larger than the bulk capacitance between the microelectrodes and thus can still affect local permittivity measurements. Moreover, capacitive stray currents to surrounding metallic parts (e.g. sample holder) may severely influence microelectrode impedance measurements by "inductive loops".[16,17]

3. Finite element calculations

In Ref. 15 it has already been discussed in detail that for two microelectrodes on adjacent grains a significant fraction of the entire current may flow on alternative pathways through neighboring grain boundaries. In case of cubic grains of identical size and identical grain boundary properties, only ≈40% of the total current passes the grain boundary in between the microelectrodes and thus a correction factor of approximately 2.5 has to be used when calculating a specific grain boundary resistivity from the measured grain boundary resistance. For spatially varying properties, current paths become non-symmetric and a simple one-to-one relation between measured grain boundary resistance and local grain boundary property is mostly not possible. In order to further quantify this aspect of "single grain boundary measurements", we employed the finite element method (Fluxexpert, Simulog, France) to calculate the grain boundary resistance statistics for given grain boundary resistivity distributions.

Two different distributions have been analyzed: (i) four grain boundary resistivities of four different orders of magnitude with a probability of 25% each; the largest and the smallest resistivity thus differ by a factor of 1000 (see Fig. 2a). (ii) Two grain boundary resistivities differing by a factor of 100 and occurring with a probability of 50% each (see Fig. 2b). In both cases, the grain boundary thickness is assumed to be constant throughout the sample. In order to simulate the expected grain boundary resistance distribution in local impedance measurements, the properties of the 20 grain boundaries in the model sample are randomly assigned to the given resistivity distribution. The dc resistance between the microelectrodes was determined from an integration of the calculated current density (see e.g. Ref. 15). The bulk resistance between the two microelectrodes was obtained from a calculation without grain boundaries ("single crystal") and subtracting this bulk resistance from the dc resistances leads to the grain boundary resistances.[15]

The grain boundary resistance distribution resulting from the *n*-fold repetition of the random assignment of grain boundary properties corresponds to the distribution to be expected when measuring n different microelectrode pairs on a sample with the given grain boundary property distribution. In Fig. 2 two calculated statistics are shown each for 40 random distributions of properties corresponding to 40 different microelectrode pairs in a hypothetical experiment. (The bars GB1–GB4 and GB1 and GB2 reflect the resistances resulting in the case of identical grain boundary resistivities in the entire sample.) In the case of four grain boundary resistivities it can be seen that not a single

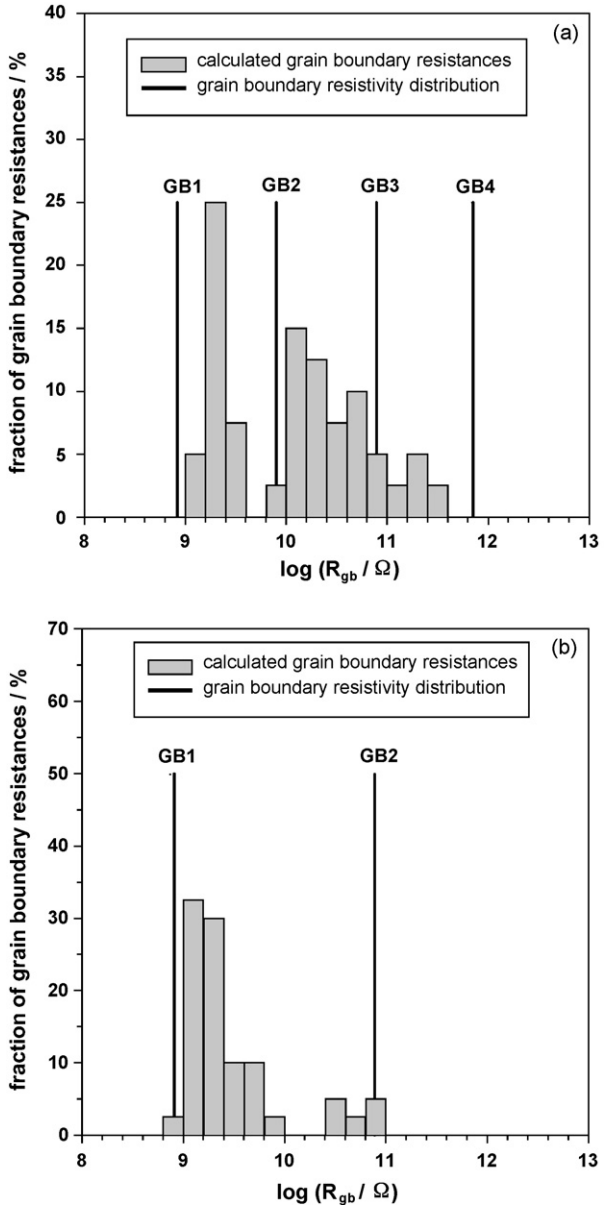

Fig. 2. Histograms of calculated grain boundary resistances between two microelectrodes for two different grain boundary resistivity distributions (a) and (b). Each histogram corresponds to hypothetical measurements on 40 different microelectrode pairs. The resistivity distributions used in the simulations are indicated by solid lines (GB1–GB4 and GB1 and GB2) at the resistances calculated for model samples with identical resistivity for all grain boundaries.

resistance corresponds to the smallest possible grain boundary resistance. This is hardly surprising since the current not only probes the grain boundary between the two microelectrodes but also sees neighboring grain boundaries as well as next near neighbors thus never being solely determined by the low resistive grain boundaries. A considerable fraction of calculated grain boundary resistances is found between the resistances of GB1 and GB2 and between GB2 and GB3. Only very few resistors indicate the existence of the highly resistive grain boundaries (GB3 and GB4). In particular not a single calculation reveals that very high resistances (GB4) are present.

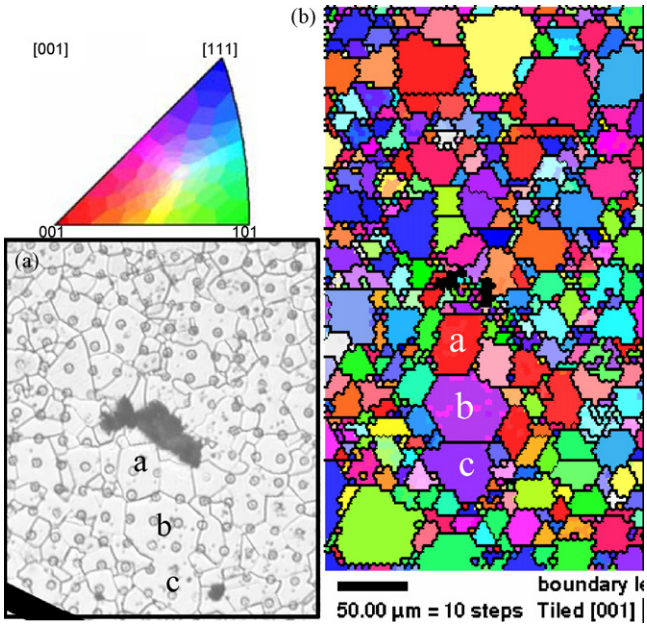

Fig. 3. (a) Polycrystalline $SrTiO_3$ with microelectrodes on the top in the optical microscope. The dark region in the center helped us to find the same region also in the OIM image. (b) OIM map of the examined area. The colors in the map indicate—via a stereographic triangle (inset)—the orientations of the grains with respect to the normal direction [0 0 1] of the sample. The letters a, b, and c in the images indicate identical grains.

This result suggests that a simple reconstruction of the true grain boundary resistivity distribution from the statistics of local grain boundary measurements (or calculations) is hardly possible and that in particular highly resistive grain boundaries can easily be overlooked or at least underestimated in their importance. On the other hand, the statistics gives an idea on the width of the distribution of medium and low resistive grain boundaries. Moreover, the existence of grain boundaries of very low resistivity is easily visible and from the measured/calculated resistance distribution their fraction may even be overestimated (though the corresponding resistances are somewhat too high due to the influence of neighboring grain boundaries). These conclusions are also in accordance with the calculations for the bimodal grain boundary resistivity distribution in Fig. 2b: the fraction of highly resistive grain boundaries is strongly underestimated while the existence of low resistive grain boundaries is easily visible in microelectrode experiments. The true resistance of GB1, however, is below the maximum of the corresponding resistance distribution.

4. Microelectrode measurements on undoped $SrTiO_3$

In order to estimate the width of the grain boundary resistivity distribution of undoped $SrTiO_3$ and to test the presence of low resistive grain boundaries, an array of $YBa_2Cu_3O_{6+x}$ microelectrodes (8 μm in diameter) was deposited on a $SrTiO_3$ polycrystal (Fig. 3a). Details on the microelectrode preparation can be found in Ref. 13. Polycrystalline $SrTiO_3$ was prepared from $SrCO_3$ (99.999%, Aldrich) and TiO_2 (99.99%, Aldrich) powders by the mixed oxide route. The mixed powder was calcined at 1375 °C under air for 1 h and isostatically pressed into a pellet under 680 MPa. The pellet was sintered under oxygen atmosphere at 1480 °C for 8 h and achieved a density of 97% of its theoretical value. Before performing impedance measurements the sample was annealed for 24 h at 600 °C in air.

At a temperature of about 320 °C 23 different microelectrode pairs on adjacent grains were then contacted by tungsten tips under the optical microscope and the impedance was measured in the frequency range 0.1 Hz–1 MHz using a Solartron 1260 frequency response analyzer with a home-made impedance converter for high impedances. A typical impedance spectrum is shown in Fig. 4 and reveals a high frequency bulk arc and a low frequency grain boundary arc in the complex impedance plane. In order to determine the resistive and capacitive elements, a fit using two serial RQ elements was performed with one RQ-element reflecting the grain boundary (gb) and the other one representing the bulk response. Symbol Q denotes a constant phase element with an impedance of $Z_Q = Q^{-1}(i\omega)^{-n}$. The equivalent circuit and the corresponding fit (solid line) are also shown in Fig. 4. In an attempt to find structure–property relations of the grain boundaries, the misorientation of neighboring grains was determined from electron back-scattered diffraction patterns (EBSD) (software program TexSEM Lab., LEO 438VP SEM). The resulting orientation imaging microscopy (OIM) map plots the different orientations of the grains (see Fig. 3b).

Fig. 5a shows the distribution of all measured grain boundary resistances in dependence of the misorientation between the two relevant grains. The following conclusions can be drawn from these measurements: (i) for none of the investigated misorientations the grain boundary resistance was particularly low; hence all grain boundaries exhibit a pronounced space charge depletion layer. (Grain boundary resistances in acceptor-doped and in nominally undoped $SrTiO_3$ are known to be caused by space charge depletion layers at grain boundaries exhibiting low hole and oxygen vacancy concentrations and thus high resistivity.[13,18,19]) This is also true for Σ3 and Σ7 boundaries found in our sample. (ii) There is no clearly visible trend in the distribution, i.e. there does not seem to be a simple relation between the grain boundary misorientation angle and the grain boundary resistance. (iii) Even though the area of the grain boundaries between the microelectrodes and thus the geometrical factor varies within these 23 measurements, the distribution of grain boundary resistances is narrow compared, for example,

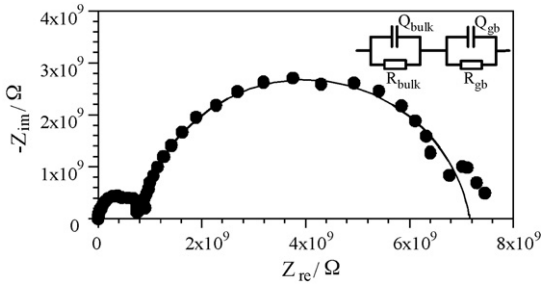

Fig. 4. (a) Impedance spectrum measured between two microelectrodes on neighboring $SrTiO_3$ grains at 320 °C including fit (solid line) to the equivalent circuit shown above.

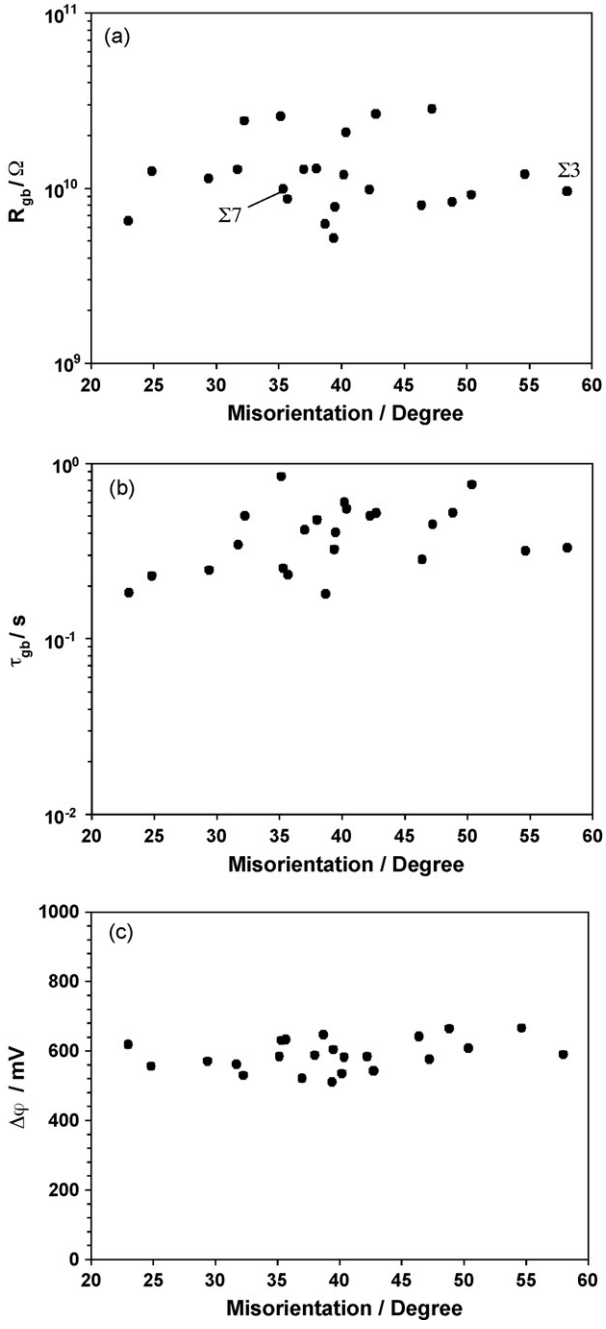

Fig. 5. (a) Distribution of the grain boundary resistances plotted versus the misorientation angle of the corresponding/neighboring grains. (b) Distribution of the grain boundary relaxation time (calculated from R_{gb} and C_{gb}, see text) plotted versus the corresponding misorientation angle. (c) Space charge potentials determined from the relaxation times of grain boundary and bulk according to Eq. (1).

to the variation of R_{gb} in Fig. 2a. Thus we conclude that grain boundary resistivities in this sample are pretty constant even though a certain fraction of very resistive grain boundaries cannot be excluded. A possible reason for the similarity of the grain boundary properties is the fact that the composition of the sample determined by induction-coupled plasma analysis as well as with X-ray energy-dispersive spectroscopy was $Sr_1Ti_{1.05}O_3$; the excess of Ti could lead to the formation of a Ti-rich amorphous secondary phase at the grain boundaries. It is also important to mention that the crystallography of a grain boundary is only partially specified by the misorientation of the neighboring grains. The orientation of the grain boundary plane (grain boundary inclination), which is not available from standard EBSD, is also a crucial parameter.

The grain boundary relaxation time can be calculated[2] from the fit data according to $\tau_{gb} = R_{gb} \cdot C_{gb}$ with $C_{gb} = (R_{gb}^{1-n} Q_{gb})^{1/n}$. Fig. 5b displays the resulting narrow distribution of the grain boundary relaxation times. The ratio of grain boundary and bulk (τ_{bulk}) relaxation time is then used to determine space charge potentials $\Delta\varphi$ with respect to the bulk potential via[2]

$$\frac{\tau_{gb}}{\tau_{bulk}} = \frac{\exp(e\Delta\varphi/kT)}{2(e\Delta\varphi/kT)}. \quad (1)$$

Symbols e, k and T denote the elementary charge, Boltzmann constant and temperature, respectively. (Please note that in Eq. (14) of Ref. 2 the ratio of relaxation frequencies should be replaced by its inverse value.) The measured "bulk" constant phase element Q_{bulk} includes contributions from the stray capacitance between the contact tips and the capacitive coupling to surrounding conducting parts of the set-up.[16] In order to get a proper bulk relaxation time the theoretical bulk capacitance between two microelectrodes $C_{bulk} = \varepsilon_0\varepsilon_r d_{me}$ instead of Q_{bulk} was thus used with ε_r being approximately 230[13] and ε_0 denoting the vacuum permittivity, respectively. It should also be noted that owing to unknown reasons the bulk resistances exhibit a significant scatter in these local impedance measurements (standard deviation of 0.44 on a logarithmic scale).

The resulting space charge potentials are shown in Fig. 5c and again support the conclusion that the electrical properties of the grain boundaries in the undoped $SrTiO_3$ ceramics are very similar; they exhibit a space charge potential of the order of 590 mV. This value is within the range of space charge potentials obtained from measurements on Fe-doped $SrTiO_3$ polycrystals and several bicrystals[13,22,20] (doping levels of the order of 10^{19} l/cm^3). In bicrystal experiments on some low angle grain boundaries and Σ3 boundaries of Fe-doped $SrTiO_3$ very low and angle sensitive grain boundary resistances were obtained[21,22] but those seem to play no role in our polycrystalline material.

5. Conclusions

Localized "single-grain boundary" impedance measurements using microelectrodes are a valuable but non-trivial tool for gaining additional information on electrical properties of polycrystalline ceramics. From an experimental point of view it is important to contact microelectrodes by tips rather than by large contact pads on the surface. Finite element calculations showed that a reconstruction of the true grain boundary resistivity distribution from the measured grain boundary resistances is hardly possible. However, some information on the width of the grain boundary resistivity distribution can be obtained from such experiments even though one should keep in mind that in case of broad distributions the fraction of low resistive grain bound-

aries is overestimated and highly resistive grain boundaries can easily be overlooked. From experiments on nominally undoped $SrTiO_3$ polycrystals a rather narrow grain boundary resistivity distribution can be concluded with space charge potentials of approximately 590 mV compared to the bulk potential. Comparison with measurements of the misorientation angle between grains does not reveal any simple structure–property relation in this material.

References

1. Greuter, F. and Blatter, G., Electrical properties of grain boundaries in polycrystalline compound semiconductors. *Semicond. Sci. Technol.*, 1990, **5**, 111–137.
2. Fleig, J., The grain boundary impedance of random microstructures: numerical simulations and implications on the analysis of experimental data. *Solid State Ionics*, 2002, **150**, 181–193.
3. Fleig, J., The influence of non-ideal microstructures on the analysis of grain boundary impedances. *Solid State Ionics*, 2000, **131**, 117–128.
4. Fleig, J. and Maier, J., Finite element calculations on the impedance of electroceramics with highly resistive grain boundaries: I. Laterally inhomogeneous grain boundaries. *J. Am. Ceram. Soc.*, 1999, **82**, 3485–3493.
5. Einzinger, R., Grain boundary properties in ZnO varistors. *Adv. Ceram.*, 1981, **1**, 359–374.
6. Tao, M., Bui Ai, Dorlanne, O. and Loubiere, A., Different single grain junctions within a ZnO varistor. *J. Appl. Phys.*, 1986, **61**, 1562–1567.
7. Olsson, E. and Dunlop, G. L., Characterization of individual interfacial barriers in a ZnO varistor material. *J. Appl. Phys.*, 1989, **66**, 3666–3675.
8. van Kemenade, J. T. C. and Eijnthoven, R. K., Direct determination of barrier voltage in ZnO varistors. *J. Appl. Phys.*, 1979, **50**, 938–941.
9. Mahan, G. D., Levinson, L. M. and Philipp, H. R., Single grain junction studies of ZnO varistors—theory and experiment. *Appl. Phys. Lett.*, 1978, **33**, 830–832.
10. Wang, H., Li, W. and Cordaro, F., Single junctions in ZnO varistors studied by current–voltage characteristics and deep level transient spectroscopy. *Jpn. J. Appl. Phys.*, 1995, **34**, 1765–1771.
11. Chung, S. Y., Kim, I.-D. and Kang, S.-J. L., Strong nonlinear current voltage behaviour in perovskite-derivative calcium copper titanate. *Nat. Mater.*, 2004, **3**, 774–778.
12. Cernik, R. J., Freer, R., Leach, C., Mongkolkachit, C., Barnes, P., Jacques, S. *et al.*, Direct correlation between ferrite structure and electrical resistivity. *J. Appl. Phys.*, 2007, **101**, 104912.
13. Rodewald, S., Fleig, J. and Maier, J., Microcontact impedance spectroscopy at single grain boundaries in Fe-doped $SrTiO_3$ polycrystals. *J. Am. Ceram. Soc.*, 2001, **84**, 521.
14. Lee, J.-S., Kim, D.-Y., Fleig, J. and Maier, J., Geometry and electrical properties of grain boundaries in Mn–Zn ferrite ceramics. *J. Am. Ceram. Soc.*, 2004, **87**, 1895–1902.
15. Fleig, J., Rodewald, S. and Maier, J., Microcontact impedance measurements of individual highly resistive grain boundaries: general aspects and application to acceptor-doped $SrTiO_3$. *J. Appl. Phys.*, 2000, **87**, 2372–2381.
16. Fleig, J., Jamnik, J., Maier, J. and Ludvig, J., Inductive loops in impedance spectroscopy caused by electrical shielding. *J. Electrochem. Soc.*, 1996, **143**, 3636–3641.
17. Lee, J.-S., Fleig, J., Maier, J., Kim, D.-Y. and Chung, T.-J., Local conductivity of nitrogen-graded zirconia. *J. Am. Ceram. Soc.*, 2005, **88**, 3067–3074.
18. Denk, I., Claus, J. and Maier, J., Electrochemical investigations of $SrTiO_3$ boundaries. *J. Electrochem. Soc.*, 1997, **144**, 3526–13526.
19. Vollmann, M. and Waser, R., Grain boundary defect chemistry of acceptor-doped titanates: high field effects. *J. Electroceram.*, 1997, **1**, 51–64.
20. Guo, X., Fleig, J. and Maier, J., Separation of electronic and ionic contributions to the grain boundary conductivity of acceptor-doped $SrTiO_3$. *J. Electrochem. Soc.*, 2001, **148**, J50–J53.
21. DeSouza, R., Fleig, J., Maier, J., Zhang, Z., Sigle, W. and Rühle, M., Electrical resistance of low-angle tilt grain boundaries in acceptor doped $SrTiO_3$ as a function of misorientation angle. *J. Appl. Phys.*, 2005, **97**, 053502.
22. Leonhardt, M., Jamnik, J. and Maier, J., In situ monitoring and quantitative analysis of oxygen diffusion through Schottky-barriers in $SrTiO_3$ bicrystals. *Electrochem. Solid State Lett.*, 1999, **2**, 333–335.